Directional growth of a smectic-A –smectic-B interface lying along a forbidden orientation

F. Melo and P. Oswald
Laboratoire de Physique, Ecole Normale Supérieure de Lyon, 46 Allée d'Italie, 69364 Lyon CEDEX 07, France
(Received 26 October 1992)

We report detailed observations of cellular growth at the smectic-A –smectic-B interface of the liquid crystal N-[4′-(n-butoxy)benzylidene]-4-(n-octyl) aniline (4O.8) when it grows along a forbidden orientation of the equilibrium shape. Four growth regimes have been observed at increasing velocity, each of them characterized by cells of a given type: symmetric cells with an angular discontinuity at the tip near the onset of instability, then partly faceted asymmetric cells forming propagating domains, followed by "chaotic" cells, and finally dendrites.

PACS number(s): 61.50.Cj, 64.70.Md

I. INTRODUCTION

In previous work [1], we reported observations of the equilibrium shape of a smectic-B germ of 4O.8 (butyloxybenzilidene octylaniline) in equilibrium with the surrounding smectic-A phase. We observed that the smectic-A –smectic-B interface has quite peculiar static properties that can be summarized as follows: the interface is faceted parallel to the smectic layers; the facet matches tangentially with the contiguous curved regions; the faces perpendicular to the layers do not occur in the equilibrium shape; and if one forces such a face to appear (for instance, in a temperature gradient), the macroscopic interface develops a hill-and-valley structure (Herring's instability) [2].

We therefore expected, and we indeed observed [3,4], that the behavior and the destabilization in directional growth of this interface depends upon its orientation with respect to the smectic layers. Thus we observed that the destabilization of a faceted interface (parallel to the layers) leads to a nonstationary crenellated structure consisting of a succession of unstable and moving macrosteps [5] and showed that attachment kinetics were responsible [6,7]. If the layers make an angle with the temperature gradient, the interface is rough on the atomic scale. At the onset of instability, cells are rounded and periodically spaced, and propagate along the macroscopic front. The diffusion anisotropy of impurity in the smectic-A phase allowed us to explain this drift [3,7].

In this article, we are interested in what happens when the front corresponds to a forbidden orientation, or more precisely, when the imposed temperature gradient is parallel to the smectic layers. Preliminary results have already been published in Refs. [3] and [4]. The main observation was that the missing orientations of the equilibrium shape are still forbidden during growth at small velocity, which leads to an angular discontinuity at the cell tip. We also observed that the low-velocity cells tend to be faceted parallel to the smectic layers.

Therefore, we wished to compare the behavior in directional growth of this special front with that of rough solid-liquid interfaces of ordinary materials such as succinonitrile or pivalic acid. We shall see that there are many similarities between our system and the others in spite of the existence of very different interfacial properties (missing orientation and faceting) which lead to cells of unusual shape. In particular, we shall see that most of the secondary bifurcations observed in classical systems are still present, which proves, once more, that they are typical of cellular fronts and relatively insensitive to the shape of the cells and to the details of the system chosen.

The organization of the article is as follows. In Sec. II, we describe the experimental apparatus. In Sec. III, we briefly describe the different growth regimes and we give the experimental bifurcation diagram. These regimes are then described in detail in Secs. IV–VII.

II. EXPERIMENT

Our experiment is known as directional solidification [8]. The sample is a thin layer of liquid crystal 4O.8 (usually 20 μm thick) that is moved at a constant pulling velocity V across a fixed temperature gradient G. The sample is sandwiched between two glass plates on which a 300-Å-thick layer of polyimide ZLI-2650 (Merck Corp.) was deposited in order to obtain a planar alignment of the molecules. This polymeric layer is further rubbed in a single direction with a point made of teflon in order to orient the smectic layers perpendicular to the microscopic scratches. Observations are made via phase-contrast microscopy. In this experiment, we freeze the smectic-A phase creating the smectic-B phase at a constant growth rate V.

III. BIFURCATION DIAGRAM

In this section, we briefly describe the different growth regimes that are observed when the experimental control parameters are changed. These parameters include the temperature gradient, the velocity, and the impurity concentration. Instead of measuring this concentration directly, we observe the corresponding freezing range $\Delta T = T_{\text{liquidus}} - T_{\text{solidus}}$, which is the important quantity in solidification. From these quantities, one can build two important lengths. The first,

$$l_D=\frac{2D_\perp}{V}\ , \tag{1}$$

is called the *diffusion length.* The quantity $D_\perp$ is the impurity diffusion coefficient in the layers, i.e., in a direction perpendicular to the director. The second,

$$l_T=\frac{\Delta T}{G}\ , \tag{2}$$

is the *thermal length.* These two lengths characterize the competition between the destabilizing effect of the diffusion field and the stabilizing effect of the temperature gradient. According to the linear analysis of Mullins and Sekerka [9], the front is unstable when these two lengths are comparable, or, more precisely, when

$$\frac{1}{l_T}=\frac{2}{l_D}\ . \tag{3}$$

This criterion of "constitutional undercooling" neglects the diffusion in the plastic smectic-B phase and surface-tension effects. The first approximation is well justified because diffusion in the Sm-A phase is faster than in the Sm-B phase by about one order of magnitude [10] so that the correction to the critical velocity $1+KD_{\text{Sm-}B}/D_{\text{Sm-}A}$, where K is the solute partition coefficient ($K\approx 0.5$[6]), is a few percent. The second approximation is also often excellent, surface tension playing a role only near the onset of absolute restabilization at very large velocity (much larger than the critical velocity). In our system, the situation is more complex because there exists, even at zero velocity, an underlying instability, caused by surface tension, that leads to a zigzag deformation of the front (Herring's instability [2]). Experimentally, the wavelength and the amplitude of this microstructure is always much smaller than the diffusion length at the onset of instability. Therefore, we can expect that the Mullins-Sekerka instability results primarily from a competition between l_D and l_T. In the following, we shall use as control parameters $1/l_{T^\alpha}G$ and $2/l_{D^\alpha}V$. In order to calculate the diffusion length, we shall use the value of $D_\perp$ that we have previously obtained in directional solidification when the interface is rough: $D_\perp\approx 6\times 10^{-7}$ cm^2/s [7]. This value was determined by measuring both the critical velocity of destabilization and the cell drift velocity as a function of the angle between the layers and the temperature gradient. As for ΔT, it was measured before and after each experiment. This precaution is necessary because the samples decompose during experiments. The purer the product, the more significant this effect is. As a rule, we rejected all the experiments during which ΔT increased by more than 10%. For this reason, the purer the sample, the shorter must be the experimental run (half an hour in the worst case when $\Delta T\approx 0.25$ °C). In the parameter plane $(1/l_T, 2/l_D)$, the "constitutional undercooling" criterion (3) is represented by a straight line of slope 1.

Let us now enumerate the different growth regimes that we observed experimentally (they will be described in detail in the following sections). At small velocity or large temperature gradient, the interface is "stable" above line 1 in the bifurcation diagram (Fig. 1). "Stability" here means that the initial Herring's structure does not change significantly. Line 1 is the critical line of destabilization of the zigzag structure. Below this line and above line 2, symmetric cells of large wavelength and amplitude (with respect to the Herring structure) develop. We note here that line 1 is slightly above the Mullins-Sekerka (MS) prediction. Between lines 2 and 3, asymmetric traveling cells, which are faceted on a single side, are seen. They form domains that compete with each other. Below line 3, the cell dynamics becomes chaotic, and the cell shape is badly defined. This regime extends down to line 4. This last limit is impossible to determine experimentally near the origin of the bifurcation diagram because there is nucleation of new germs of smectic-B phase ahead of the moving interface. This phenomenon has been studied in Ref. [5]. Nevertheless, it is possible to observe dendrites on the purest samples in the right part of the bifurcation diagram, below line 4.

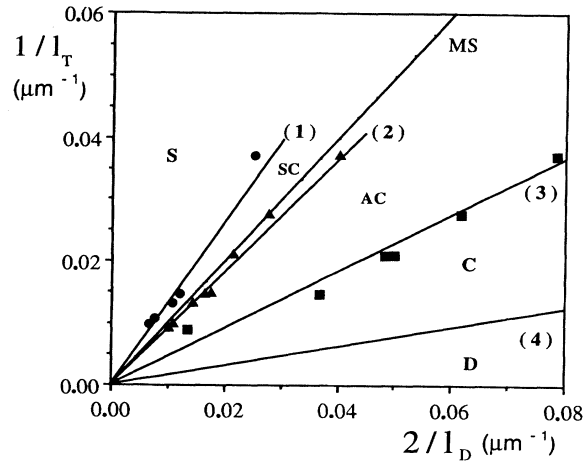

FIG. 1. Bifurcation diagram. $l_T=\Delta T/G$ and $l_D=2D_\perp/V$ are, respectively, the thermal length and the diffusion length (given in μm). The solid lines (1)–(4) separate different regimes of growth: S, stable interface; SC, symmetric cells; AC, asymmetric cells; C, chaotic cells; D, dendrites. The MS line (Mullins-Sekerka line) corresponds to the constitutional undercooling criterion ($1/l_T=2/l_D$).

IV. DESTABILIZATION OF HERRING'S STRUCTURE: SYMMETRIC CELLS

We have already described this bifurcation in Ref. [2]. Figure 2(a) shows the Herring microstructure just before destabilization. By increasing slowly the velocity, it is possible to determine a critical velocity V_1 (line 1 in Fig. 1) above which isolated triangular structures develop [Fig. 2(b)]. These triangles grow and join to form unusual "brace"-shaped cells with an angular discontinuity at the tip, while the grooves between them are somewhat faceted [Fig. 2(c)]. This cellular bifurcation is subcritical because there is an important jump in amplitude at the onset. Also, there is hysteresis, the large-amplitude cells

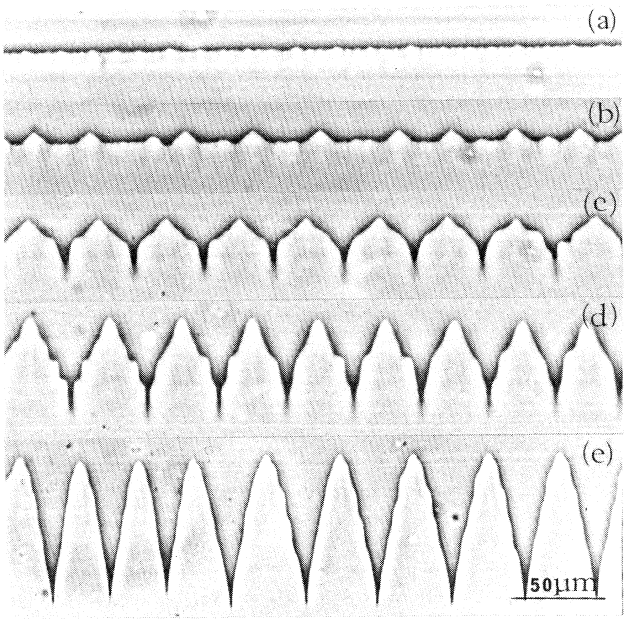

FIG. 2. Destabilization of Herring's hill-and-valley structure. Near the onset of instability, the cells are symmetric and show an angular discontinuity at the tip with lateral modulations of small amplitude which are spatially coherent over about ten cells. $\Delta T \approx 0.7\,^{\circ}\mathrm{C}$ and $G = 76\,^{\circ}\mathrm{C/cm}$. (a) $V = 0.2\ \mu\mathrm{m/s}$; (b) and (c) $V = 0.38\ \mu\mathrm{m/s}$; (d) $V = 0.4\ \mu\mathrm{m/s}$; (e) $V = 0.45\ \mu\mathrm{m/s}$.

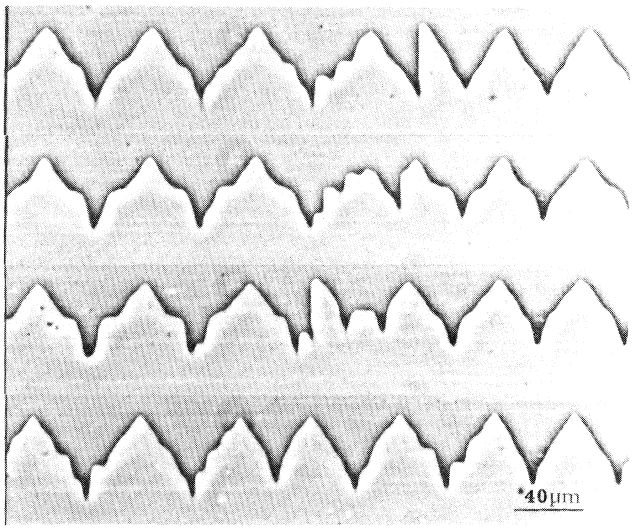

FIG. 3. Disappearance of an isolated asymmetric cell which has formed accidentally in an array of symmetric cells. This sequence shows the stability of the symmetric cells near the onset of instability with respect to the asymmetric faceted cells. $\Delta T \approx 1\,^{\circ}\mathrm{C}$, $G = 76\,^{\circ}\mathrm{C/cm}$, and $V = 0.25\ \mu\mathrm{m/s}$.

disappearing again only for a velocity 15–20 % smaller than V_1. The fact that V_1 is slightly smaller than the theoretical prediction (line 1 is above the MS line in the bifurcation diagram) is doubtless due to the existence of a small initial deformation of the front (the Herring microstructure) which increases the destabilizing effect of the diffusion field. It is indeed well known in directional solidification that a polycrystal destabilizes first near the grooves that develop at the intersections between the interface and the grain boundaries [11]. If one increases the velocity, the cell amplitude increases very rapidly while lateral undulations occur [Figs. 2(d) and 2(e)]. As we shall see in Sec. V, these modulations have nothing in common with the side branches of dendrites. For this reason, we guess that they are due to the large surface-tension anisotropy of our system [1] and to the tendency of smectics to facet parallel to the layers. Another important observation is that these side undulations are correlated across many cells when the diffusion length is much larger than the cell spacing. Unfortunately, the mechanism by which correlations occur is still unclear. In particular, it was never possible to see oscillations (transverse or longitudinal) of the cell tips as certain theoretical models have suggested [12]. Finally, we would like to insist on the stability of these symmetric cells, even if their domain of existence in the parameter plane is rather small experimentally (see Fig. 1). Indeed, it can happen that a faceted asymmetric cell (similar to those described in the next section) comes in between two symmetric cells. In this case, it becomes symmetric again rapidly by local rearrangements with its nearest neighbors (Fig. 3). On the other hand, if the velocity exceeds a second threshold V_2, asymmetric cells invade the whole sample.

V. FIRST SYMMETRY BREAKING: ASYMMETRIC CELLS ORGANIZED IN DOMAINS

A. Bifurcation

Above a second critical velocity V_2 (line 2 in the phase diagram of Fig. 1), symmetric cells are unstable because of their tendency to pin facets on the side. This pinning occurs preferentially in the grooves of the widest cells and leads to new cells whose tips are always warmer than those of symmetric cells. These cells, initially narrow, widen while remaining asymmetric [Fig. 4(a)]. This widening is amplified by their drift motion along the macroscopic interface. The motion is due to the growth of the facet and is related generically to the symmetry breaking of the cellular pattern. It has been observed in other experiments of solidification [13], in a directional-fingering experiment [14], and in a wetting experiment [15]. The drift motion has another important consequence on front dynamics since it leads to the nucleation of a source of cells [Fig. 4(b)]. Indeed, the propagating cell "swallows" the symmetric cell that is adjacent to its faceted side while a new asymmetric cell, of opposite sign (i.e., faceted on the other side), develops from the groove of the mother cell. This mechanism leads to the total disappearance of the symmetric cells and to the structuring of the cellular pattern into domains of opposite signs separated by sources and sinks of cells (Fig. 5). In the following, we shall call domains or cells "+" ("−") if the facet is on the right (left). Experimentally, the exact determination of V_2 is difficult because the transient regime is sometimes very long (several hours). In particular, the less pure the sample, the longer is the transient.

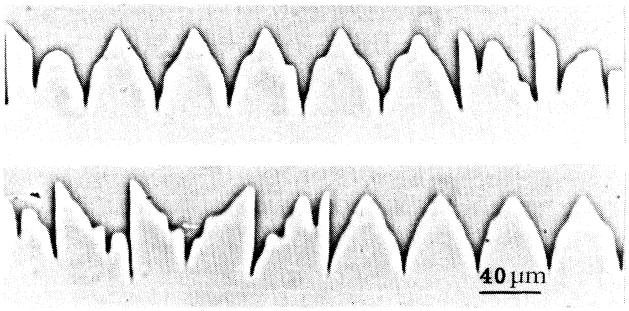

FIG. 4. Nucleation of asymmetric cells in an array of asymmetric cells. Facets are pinned preferentially in the grooves of the widest cells. The tip of the faceted cells is always warmer than that of the symmetric cells. In (a), two neighboring cells have transformed simultaneously into asymmetric cells of the same sign. In (b), the transformation occurred by successive nucleation of two asymmetric cells of opposite signs. A source of asymmetric cells is born.

For this reason, we have taken for critical velocity V_2 (line 2 in Fig. 1) that for which the percentage of asymmetric cells exceeds 10% after a time equal to the diffusion time $D_\perp/KV^2$ (K is the impurity partition coefficient). We also checked that it was necessary to decrease the velocity at least 15% below V_2 to observe again the total disappearance of the asymmetric cells. This hysteresis is the signature of a subcritical bifurcation.

B. Domain dynamics

In this subsection, we describe how domains compete with each other. We place ourselves in the asymmetric cell (AC) region of the phase diagram.

Figure 5 shows the evolution in time of a − domain limited by two + domains. The "wall" between two domains is a sink if the two domains approach and a source if they move away. In this figure, the sink is quasimotionless during the observation time (about 2 min) whereas the source moves to the left. For this reason, the − domain, in which the wavelength is on average slightly larger than in its two neighbors, becomes narrower. As a general rule, the domain having the smaller wavelength grows at the expense of that of larger wavelength.

The competition between domains is a local phenomenon that takes place near the walls. Indeed, if one looks attentively at the cell nucleation in a source (Fig. 5), one sees that the last cell of the + domain generates a − cell and vice versa. Therefore, if each domain yields the same number of cells as its neighbor per unit time, the source is motionless. By contrast, the source drifts if a domain becomes more productive than the other, a phenomenon that occurs as soon as the wavelengths are different. Thus, in Fig. 5, cells of large wavelength are more productive than the others, which leads to their progressive disappearance. The situation is rather different in a sink. The cellular death can occur in two different ways: either two cells of opposite signs disappear simultaneously or they disappear alternately. This second situation is by far the most common (Fig. 5): in this case, the cell disappearing first weakens its neighbor of opposite sign which disappears during the next collision. As long as this process is repeated, the sink does not move as observed in Fig. 5. A sink displacement happens when a cell slightly higher than the average succeeds in surviving two successive collision at least.

Finally, one observes that there exists a wavelength gradient along a given domain, cells being a little larger near a source than in the vicinity of a sink. Thus the size

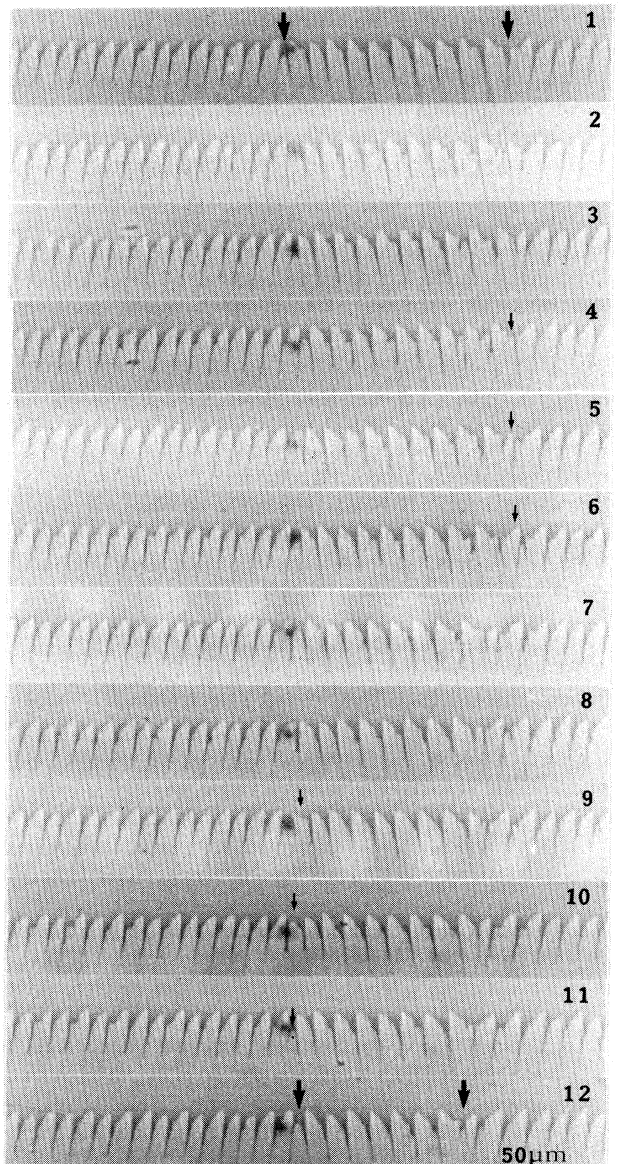

FIG. 5. Source and sink of cells in the asymmetric regime (thick arrows in the photographs). $\Delta T \approx 0.23\,^\circ$C, $G = 63\,^\circ$ C/cm, and $V = 2.5$ μm/s. The time interval between two successive photographs is 10 s. By convention, cells (+) [(−)] have their facet and drift on the right (left). The small arrows in photos (4–6) show the birth of a cell (+) on the nonfaceted side of a cell (−). The arrows (9–11) show the progressive disappearance of a cell (−) in a sink.

of a cell changes during its motion, which indicates a phase diffusion. This phenomenon brings us to the study of the wavelength selection.

C. Wavelength selection

There are three mechanisms that allow us to adjust the wavelength: sources and sinks of cells, phase diffusion, and development of side branches. A convenient method to study these phenomena is to change abruptly the pulling velocity. Of course, the initial and final velocities (V_i and V_f in the following) are chosen in order to stay in the same AC region of the bifurcation diagram (Fig. 1).

If the jump in velocity is large ($V_f \approx 2V_i$), the domains break up because of the local development of side branches on the rough side of the cells. The larger the wavelength, the more efficient is this instability. This mechanism leads to a new cell of opposite sign which forms with the previous one a new source of cells. If V_f is large enough one also observes tip splitting. In this case, the cell divides into two cells of the same sign. This stage leads quickly to a large number of sinks and sources separated by domains of small size. These domains can then compete and grow as previously described. The phase diffusion plays in that case an important role.

If the jump in velocity is small, side branching cannot develop. The wavelength adjustment is then much slower than before and depends only on the sources that supply narrower cells, on cellular death in the sinks and on the phase diffusion. It is also common to observe cells keeping the same wavelength for a long time: in this case they transiently develop side branches. But their amplitude is never sufficient to lead to a new cell.

Inversely, one can observe the result of starting from a high velocity and reducing it abruptly. In this case, the narrowest cells start to lag behind the others and then are choked off by their two neighbors. This mechanism of cell death is common in most materials [16]. The following step is slow, through the sources and sinks and the phase diffusion. If the jump in velocity is small, we never observe cell death outside the sinks between domains.

In conclusion, the wavelength adjustment brings into play very different characteristic times. One can distinguish short times corresponding to the development of a side branch or the splitting of a cell tip. These times are shorter than the diffusion time. Another time is that corresponding to the disappearance or the nucleation of a cell in a sink or a source separating two domains. This time is determined by the drift velocity V_d of the cells and their wavelength λ: it is equal to λ/V_d and is in general comparable to the diffusion time. Finally, one must consider a much longer time that is associated with the phase diffusion. This time depends on the drift-velocity gradient and on the domain size and is at least ten times larger than the diffusion time.

D. Drift velocity and wavelength measurements

In Fig. 6 we plot the average drift velocity of the asymmetric cells as a function of the growth rate for samples of different ΔT and for a fixed temperature gradient. We

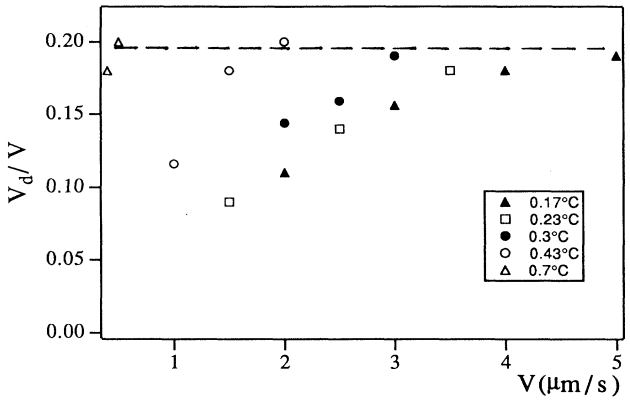

FIG. 6. Drift velocity (normalized to the pulling velocity) vs growth velocity. Each symbol corresponds to a sample of a given purity (the corresponding freezing range ΔT is indicated beside each symbol in the graph). One notes that V_d/V tends to 0.2, a value that is independent of the sample chosen.

observed that V_d has always a finite value at the symmetrical-asymmetrical transition. Moreover, V_d increases with velocity and tends to $0.2V$ for all the samples. This limiting value of V_d/V, close to 0.2, marks clearly the transition towards chaos (see the following section). This measurement is not the only one to announce a change in the dynamics of the cellular pattern.

Indeed, we also measured the mean wavelength λ and its relative dispersion σ/λ as a function of the pulling velocity [Fig. 7(a)] as well as the position of the cell tips in

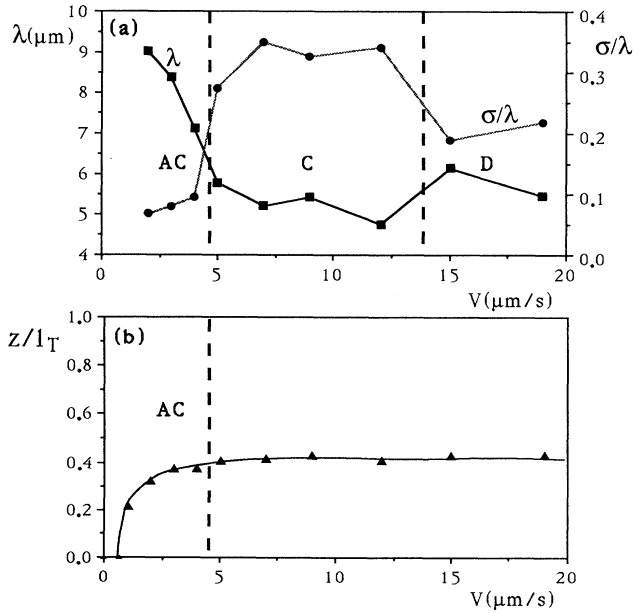

FIG. 7. (a) Mean wavelength λ and its relative dispersion σ/λ vs growth velocity. (b) Position of the cell tips, normalized to the thermal length $l_T = \Delta T/G$, vs growth velocity. $\Delta T \approx 0.17$ °C, $G = 63$ °C/cm, and $l_T \approx 27$ μm. The average position of the front before destabilization defines the origin $z = 0$. The tips of the cells cease to advance into the hot regions as soon as the chaotic regime has been reached.

the temperature gradient [Fig. 7(b)]. For measuring the tip temperature we used the double-sample method already described in Ref. [5]. This method allows us to measure temperature variations with an accuracy of 0.01 °C much more easily than with a thermocouple. The first observation is that the wavelength is well defined (within about 10%) and strongly decreases with velocity in the AC regime. By contrast, wavelength changes little in the chaotic regime and shows a large dispersion. The second observation is that the cell tip temperature steadily increases from T_{solidus} to $T_{\text{solidus}}+0.4\Delta T$, then saturates at this value for higher velocities.

Therefore, as for the drift velocity, the wavelength and the tip temperature both show a drastic change in behavior when the velocity exceeds a certain limit V_3 represented by line 3 in the phase diagram (Fig. 1). This limit corresponds to a transition towards a chaotic behavior that we now describe.

VI. CHAOTIC REGIME

When the velocity exceeds a critical value V_3 (line 3 in the phase diagram), the tip of the cells start to split frequently (Fig. 8) while side branches develop. As a consequence the domains of asymmetric cells disappear very quickly. These instabilities are not transient and affect all the cells. Cell death is also frequently observed. Note that during tip splitting, the angular discontinuity at the cell tip disappears transiently. Thus the tip is rounded during a short moment and is completely out of thermodynamical equilibrium. These local instabilities lead to a chaotic behavior and to cells of irregular shape. Chaos is clearly made evident by plotting the spatiotemporal diagram of the front. Such a diagram is obtained using video recording and digitizing at fixed intervals video lines perpendicular to the pulling velocity and intersecting cell grooves. These lines are then replotted sequentially to give an x-t picture of the pattern's evolution. The diagram obtained just after a jump in velocity (from V_{AC} in the asymmetric cells regime to V_C in the chaotic regime) is pictured in Fig. 9. It shows that chaos occurs after a time comparable to the diffusion time.

It is also possible, when chaos has occurred, to decrease again the velocity (from V_c to V_{AC}). In this case (Fig. 10), the interface evolution is quite different. Wider asymmetric cells form first randomly along the interface. Their tip is often a bit warmer than that of their neighbors. Then these cells drift along the interface, creating new asymmetric cells while the old ones progressively disappear. This step of the process is at least ten times slower than the first one. After a time of the order of $10D_{\perp}/KV^2$, domains have reappeared with a wavelength 10–20 % larger than that we would obtain by increasing progressively the velocity from zero.

Finally, we again emphasize the large dispersion of the wavelength in this regime (Fig. 7) as well as its relative constancy with velocity. The tip temperature is also independent of the velocity, by contrast with the preceding regime.

VII. DENDRITES

Above a new threshold in velocity (V_4 in the following, corresponding to line 4 in the bifurcation diagram of Fig. 1), another regime occurs. It is accompanied by a slight increase of the wavelength and, more importantly, by a sudden decrease of its dispersion (Fig. 7). Cells are again well defined (Fig. 11) and resemble classical dendrites with well-developed side branches. They are symmetric too and, consequently, they do not propagate along the

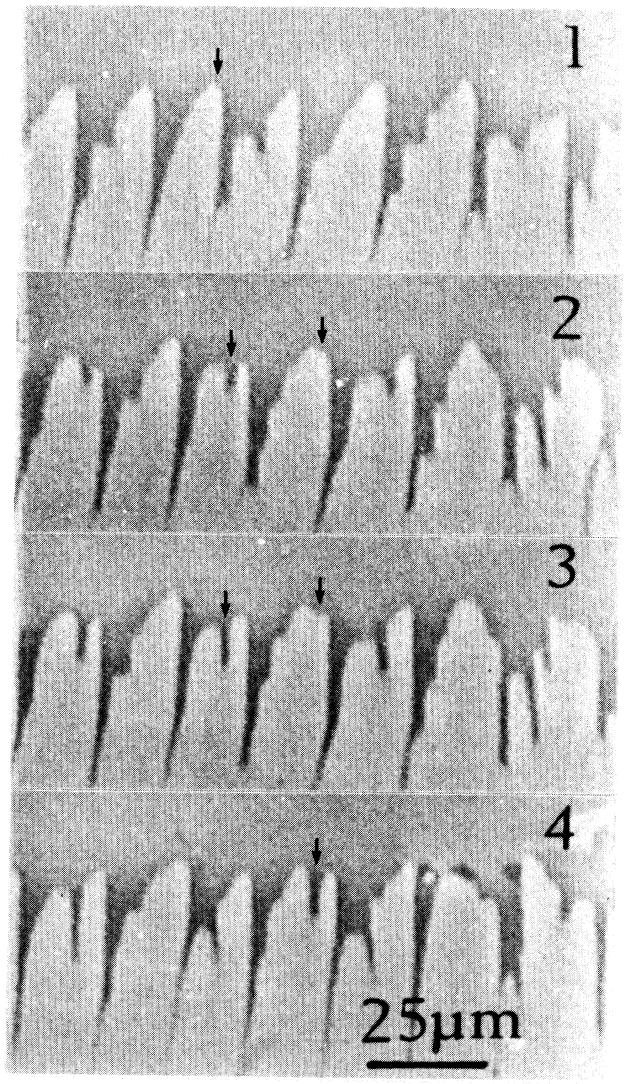

FIG. 8. Tip splitting of the asymmetric cells leading to a chaotic state where the mean wavelength is badly selected. In this nonstationary regime, cells have various shapes and can be symmetric or not with large facet. They change form continually by tip splitting. The photographs have been taken at $t=0(1)$, $t=16$ s (2), $t=20$ s (3), and $t=32$ s (4). $\Delta T\approx 0.3$ °C, $G=63$ °C/cm, and $V=3$ μm/s.

front. In this regime the wavelength varies with velocity as $V^{-0.4}$ [4] and changes by local growth of side branches or by cell death. On the other hand, tip splitting is never observed. Finally, the side branching amplitude tends to decrease with velocity, leading to narrow and very pointed cells at very large velocity (Fig. 12). In this case the wavelength dispersion seems to increase again: this is partly due to the side branching disappearance, but also to an experimental artefact, namely the existence of a longer and longer thermal transient comparable, at the largest usable velocities (≈ 200 μm/s), to the whole duration of the experiment. These phenomena can only be observed in very pure samples; otherwise, nucleation occurs ahead of the interface and breaks up the cellular pattern.

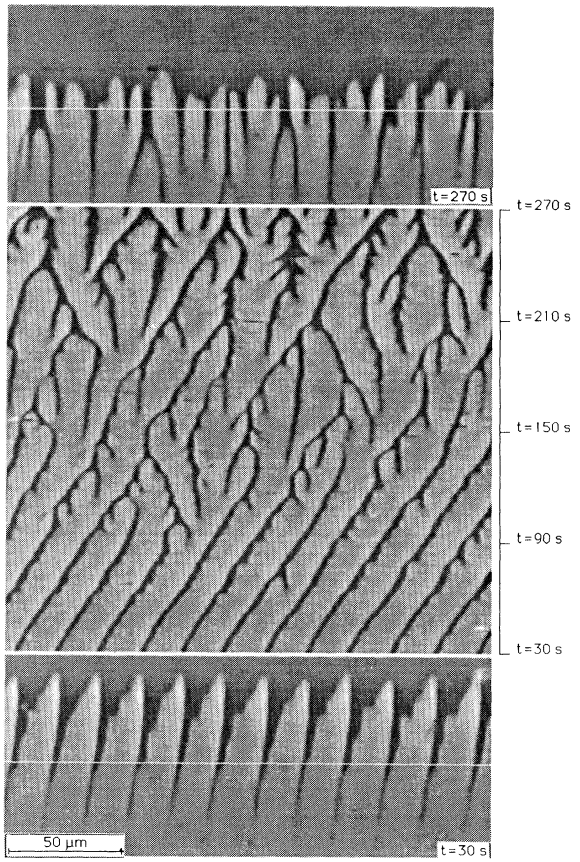

FIG. 9. Spatiotemporal diagram showing the forming of the chaotic regime. At time $t=0$, the velocity has jumped from $V=1.5$ μm/s (domain regime) to $V=2.5$ μm/s (chaotic regime). $\Delta T \approx 0.4$ °C, $G=63$ °C/cm. Time is indicated on the right of the diagram which starts 30 s after the jump in velocity. The two photographs show the cellular pattern at the beginning and at the end of the sequence. The white line on each photograph marks the position of the digitalized video line. Note that its position, fixed in the frame of the laboratory, has changed with respect to the tip of the cells. This effect is mainly due to the unavoidable shift of the temperature gradient when the velocity changes.

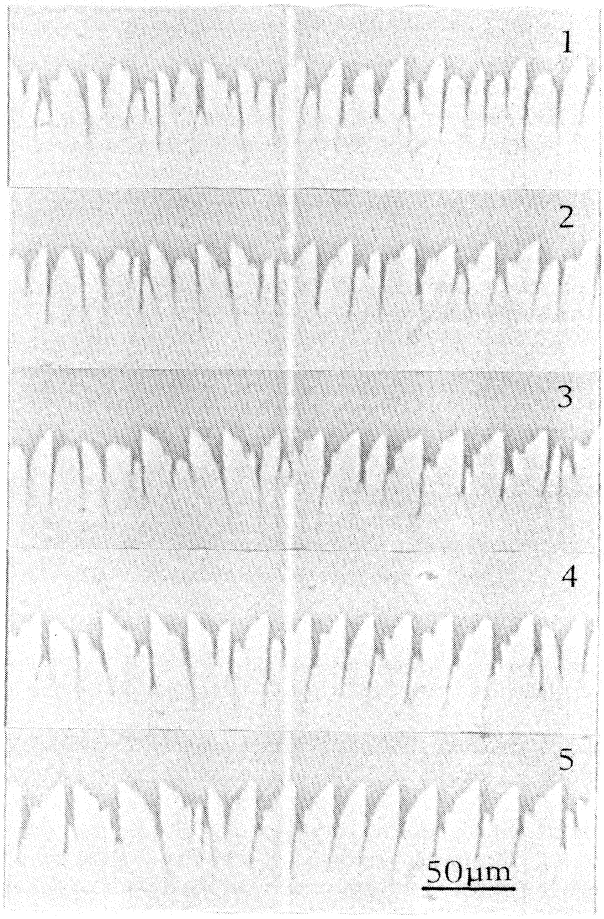

FIG. 10. Sequence of pictures showing the passage from the chaotic regime to the asymmetric one after a jump in velocity from $V=3.2$ to 2 μm/s at $t=0$. All these pictures have been taken at $V=2$ μm/s and at times $t=10$ s(1), $t=25$ s(2), $t=36$ s (3), $t=52$ s (4), and $t=85$ s (5). In (5), the domains of asymmetric cells are again clearly visible. For this sample, $\Delta T \approx 0.33$ °C, $G=63$° C/cm, and $V_3 \approx 2.9$ μm/s.

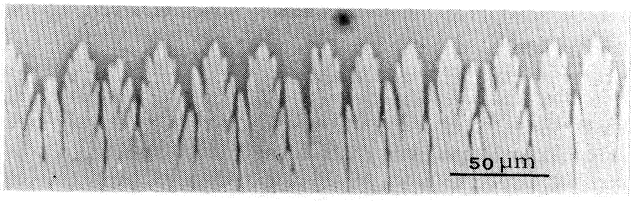

FIG. 11. In the dendritic regime, the cells are again symmetric and show side branches of large amplitude. The wavelength is also well defined [see Fig. 7(a)] and adjusts itself after a jump in velocity either by cell death or by growth of side branches. By contrast with the chaotic regime, we no longer observe tip splitting at large velocity. Because of nucleation ahead of the interface in this sample, it was impossible to observe the front behavior at larger velocity (see Fig. 12). $\Delta T \approx 0.23$ °C, $G=63$ °C/cm, and $V=7$ μm/s.

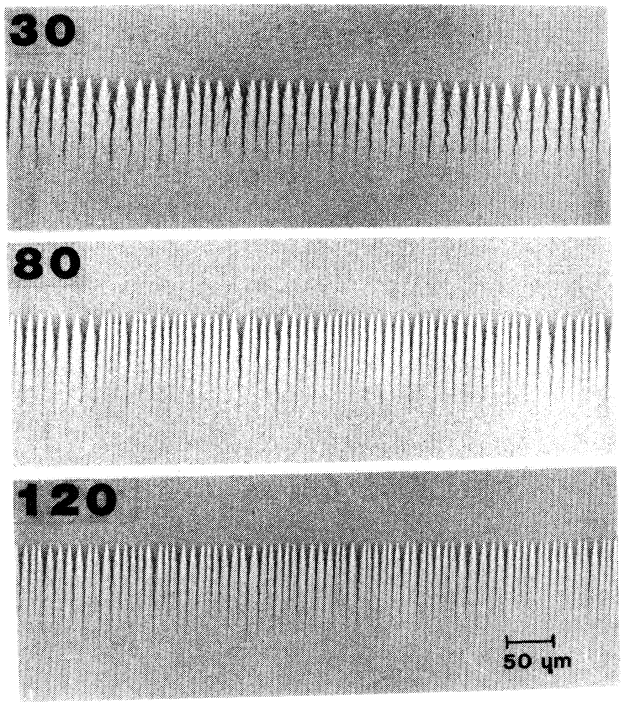

FIG. 12. Evolution at "very" large pulling velocity of dendrites. This sequence of pictures from Ref. [4] has been made with another sample of 4O.8 (another synthesis) and a different surface treatment of the glass plates. For reasons that we cannot explain, nucleation was much less important in this old experiment. $G = 90\,^{\circ}\mathrm{C/cm}$ and $\Delta T \approx 0.27\,^{\circ}\mathrm{C}$ (this value has been estimated *a posteriori* from the critical velocity measured experimentally). The velocity in μm/s is printed on the upper-left-hand corner of the photographs.

VIII. CONCLUSION

We have observed four growth regimes of the smectic-B–smectic-A interface in planar samples of the liquid crystal 4O.8. The front is oriented along a forbidden orientation of the equilibrium shape.

Up to a critical velocity V_1, which is slightly smaller than that given by the "constitutional undercooling" criterion, Herring's hill-and-valley microstructure does not change significantly.

Above V_1, and in a small range of velocity, symmetric cells with both an angular discontinuity at the tip and small-amplitude lateral modulations develop. This peculiar shape of the cells is clearly related to the existence of missing orientations and facets in the equilibrium shape of a smectic-B monocrystal. The cellular bifurcation is subcritical.

Above a second threshold V_2, asymmetric faceted cells forming drifting domains occur. These domains are separated by sources and sinks in which cells are born and die. The cell spacing is rather well selected in this regime because of the cell motion. It would be interesting to know which effect, surface-tension anisotropy or attachment kinetics, is the more important for determining the facet size and the drift velocity. Numerical simulations such as those of A. Bedda and Ben Amar on partly faceted cubic crystals [17] should give valuable information about this point.

If the velocity is further increased and exceeds V_3, tip splitting occurs and leads to a chaotic state. The shape of the cells is then badly defined with a broad distribution of wavelengths about a mean value that varies little with velocity. From this point of view, this regime resembles the predendritic regime that is observed in usual materials [18]. On the other hand, it is interesting to consider tip splitting because it is generally accepted that materials with a large surface-stiffness anisotropy do not split easily [16].

At velocity larger than V_4, pointed dendrites with large-amplitude side branches occur. In this regime the wavelength is again well selected and larger than in the chaotic regime just at the transition. This increase of the mean cell spacing at the cell-to-dendrite transition is also observed in usual materials [19]. In this regime, tip splitting is never observed. By contrast, side branches can eventually give rise to new cells, a phenomenon that has been observed in other materials [16] and in numerical simulations [20]. When the velocity increases, the side branching tends to disappear, which makes the wavelength adjustment more difficult. Nevertheless, further experiments are required to know whether there is a new dendrite-to-cell transition near the limit of absolute stability as has been observed in a carbon-tetrabromide system [21].

Finally, we mention that work on rapid solidification of thin-film silicon single crystals [22] has shown that the wavelength is selected by tip splitting of the faceted cells. Theory suggests that this process occurs when the kinetic undercooling at the cell tip becomes zero [23]. At this moment, the facet ceases growing near the tip, which spontaneously splits. A similar mechanism is perhaps responsible for the tip splitting of the cells in the chaotic regime. This interpretation is reinforced by the fact that the tip temperature stops increasing as soon as the chaotic regime is reached.

ACKNOWLEDGMENTS

We thank J. C. Géminard for fruitful discussions. This work was partly supported by DRET Contract No. 92/1313/DS/SR.

[1] P. Oswald, F. Melo, and C. Germain, J. Phys. (Paris) **50**, 3527 (1989).
[2] F. Melo and P. Oswald, Ann. Chim. Fr. **16**, 167 (1991).
[3] F. Melo and P. Oswald, Phys. Rev. Lett. **64**, 1381 (1990).
[4] J. Bechhoefer, P. Oswald, A. Libchaber, and C. Germain, Phys. Rev. A **37**, 1691 (1988).
[5] F. Melo and P. Oswald, J. Phys. (Paris) II **1**, 353 (1991).
[6] P. Oswald and F. Melo, J. Phys. (Paris) II **2**, 1345 (1992).
[7] F. Melo, thèse de Doctorat, Université Claude Bernard-Lyon I, 1991.

[8] K. A. Jackson and J. D. Hunt, Acta. Metal. **13**, 1212 (1965).
[9] W. W. Mullins and R. F. Sekerka, J. Appl. Phys. **35**, 444 (1965).
[10] G. J. Krüger, Phys. Rep. **82**, 230 (1992).
[11] S. C. Hardy, G. B. McFadden, S. R. Coriell, P. W. Voorhees, and R. F. Sekerka, J. Cryst. Growth **114**, 467 (1991).
[12] A. Karma and P. Pelcé, Phys. Rev. A **39**, 4162 (1989).
[13] A. J. Simon, J. Bechhoefer, and A. Libchaber, Phys. Rev. Let. **61**, 2574 (1988); P. Oswald, J. Phys. (Paris) II **1**, 571 (1991); F. Heslot and A. Libchaber, Phys. Scr. **T9**, 126 (1985); R. Trivedi, Appl. Mech. Rev. **43**, S79 (1990); J. T. Gleeson, P. L. Finn, and P. E. Cladis, Phys. Rev. Lett. **66**, 236 (1991); S. de Cheveigné and C. Guthmann, J. Phys. (Paris) I **2**, 193 (1992); G. Faivre, S. de Cheveigné, C. Guthmann, and P. Kurowski, Europhys. Lett. **9**, 779 (1989); J. Mergy, thèse de Doctorat, Université de Paris VI, 1992.
[14] S. Michalland, thèse de Doctorat, Université de Paris VI, 1992; M. Rabaud, S. Michalland, and Y. Couder, Phys. Rev. Lett. **64**, 184 (1990).
[15] F. Melo (unpublished).
[16] J. Bechhoefer and A. Libchaber, Phys. Rev. B **35**, 1393 (1987).
[17] A. Bedda and M. Ben Amar, Phys. Rev. A **43**, 5702 (1991).
[18] P. Kurowski, thèse de Doctorat, Université de Paris VI, 1990; P. Kurowski, C. Guthmann, and S. de Cheveigné, Phys. Rev. A **42**, 7368 (1990).
[19] M. A. Eshelman, V. Seetharaman, and R. Trivedi, Acta Metall. **36**, 1165 (1988).
[20] C. Misbah, H. Müller-Krumbhaar, and Y. Saito, J. Cryst. Growth **99**, 156 (1990).
[21] R. Trivedi, J. A. Sekhar, and V. Seetharaman, Metal. Trans. **20A**, 769 (1989).
[22] M. W. Geis, H. I. Smith, D. J. Silversmith, R. W. Mountain, and C. W. Thomspon, J. Electrochem. Soc. **130**, 1178 (1983); L. Pfeiffer, S. Paine, G. H. Gilmer, W. van Saarloos, and K. W. West, Phys. Rev. Lett. **54**, 1944 (1985); D. Dutartre, Mat. Res. Symp. Proc. **107**, 157 (1988).
[23] D. K. Shangguan and J. D. Hunt, Mat. Res. Symp. Proc. **107**, 175 (1988); D. K. Shangguan and J. D. Hunt, J. Cryst. Growth **96**, 856 (1989).

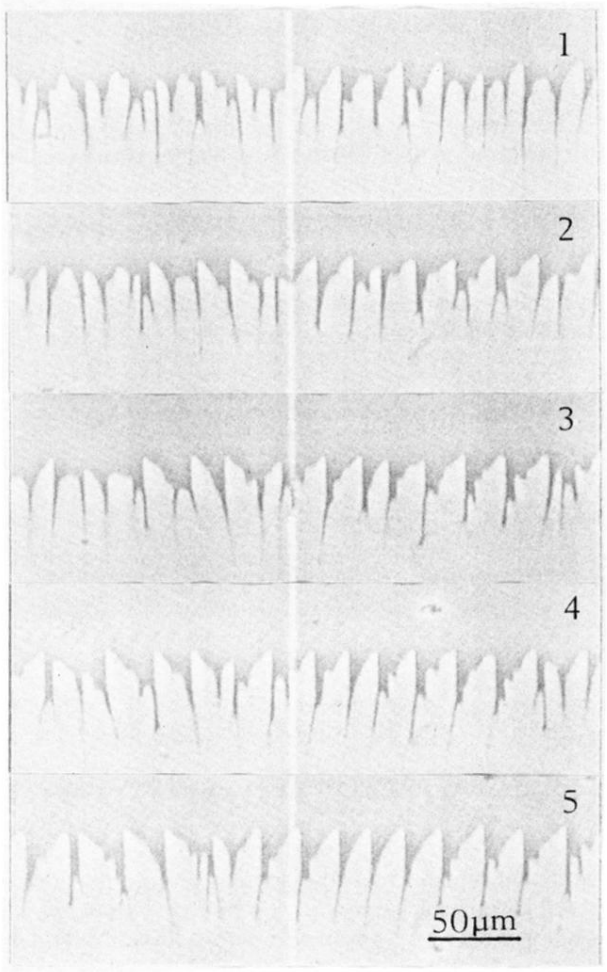

FIG. 10. Sequence of pictures showing the passage from the chaotic regime to the asymmetric one after a jump in velocity from $V=3.2$ to 2 μm/s at $t=0$. All these pictures have been taken at $V=2$ μm/s and at times $t=10$ s(1), $t=25$ s(2), $t=36$ s (3), $t=52$ s (4), and $t=85$ s (5). In (5), the domains of asymmetric cells are again clearly visible. For this sample, $\Delta T\approx 0.33$ °C, $G=63$° C/cm, and $V_3\approx 2.9$ μm/s.

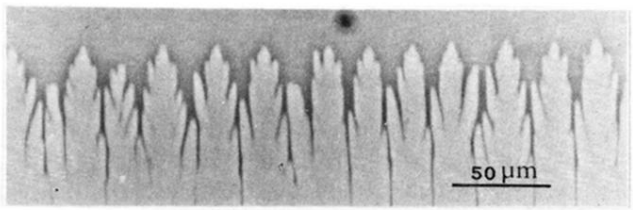

FIG. 11. In the dendritic regime, the cells are again symmetric and show side branches of large amplitude. The wavelength is also well defined [see Fig. 7(a)] and adjusts itself after a jump in velocity either by cell death or by growth of side branches. By contrast with the chaotic regime, we no longer observe tip splitting at large velocity. Because of nucleation ahead of the interface in this sample, it was impossible to observe the front behavior at larger velocity (see Fig. 12). $\Delta T \approx 0.23\,^{\circ}\mathrm{C}$, $G = 63\,^{\circ}\mathrm{C/cm}$, and $V = 7\,\mu\mathrm{m/s}$.

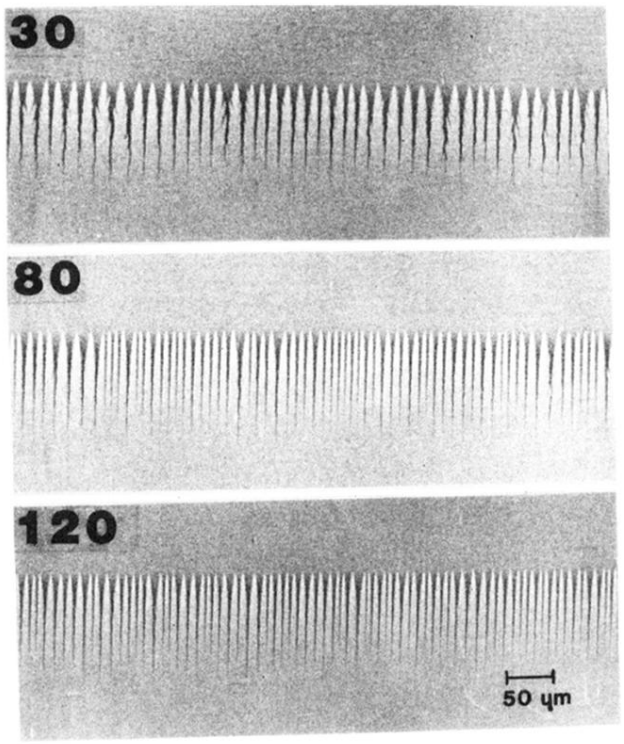

FIG. 12. Evolution at "very" large pulling velocity of dendrites. This sequence of pictures from Ref. [4] has been made with another sample of 4O.8 (another synthesis) and a different surface treatment of the glass plates. For reasons that we cannot explain, nucleation was much less important in this old experiment. $G = 90\,^{\circ}\mathrm{C/cm}$ and $\Delta T \approx 0.27\,^{\circ}\mathrm{C}$ (this value has been estimated *a posteriori* from the critical velocity measured experimentally). The velocity in μm/s is printed on the upper-left-hand corner of the photographs.

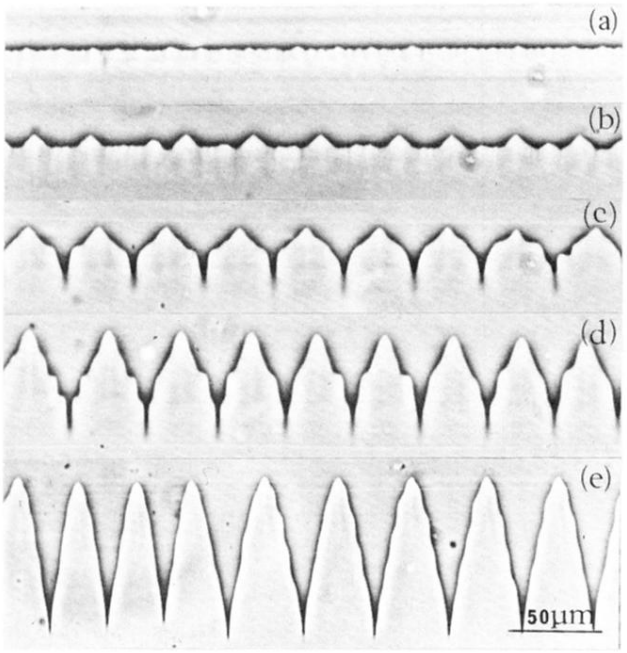

FIG. 2. Destabilization of Herring's hill-and-valley structure. Near the onset of instability, the cells are symmetric and show an angular discontinuity at the tip with lateral modulations of small amplitude which are spatially coherent over about ten cells. $\Delta T \approx 0.7\,^{\circ}\mathrm{C}$ and $G = 76\,^{\circ}\mathrm{C/cm}$. (a) $V = 0.2\ \mu\mathrm{m/s}$; (b) and (c) $V = 0.38\ \mu\mathrm{m/s}$; (d) $V = 0.4\ \mu\mathrm{m/s}$; (e) $V = 0.45\ \mu\mathrm{m/s}$.

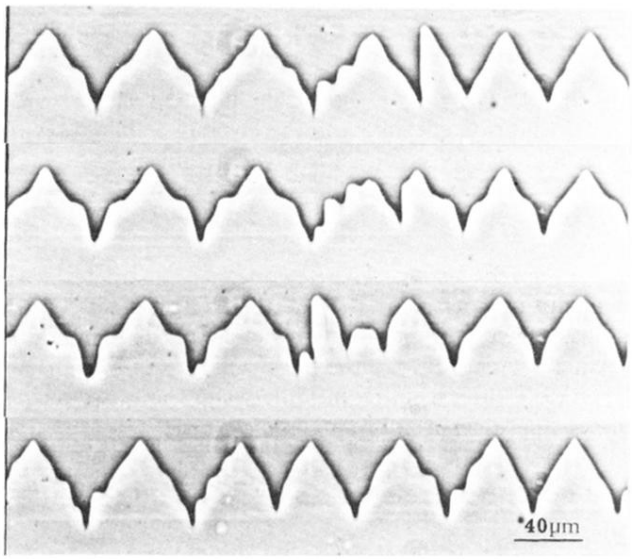

FIG. 3. Disappearance of an isolated asymmetric cell which has formed accidentally in an array of symmetric cells. This sequence shows the stability of the symmetric cells near the onset of instability with respect to the asymmetric faceted cells. $\Delta T \approx 1\,^{\circ}\mathrm{C}$, $G = 76\,^{\circ}\mathrm{C/cm}$, and $V = 0.25\,\mu\mathrm{m/s}$.

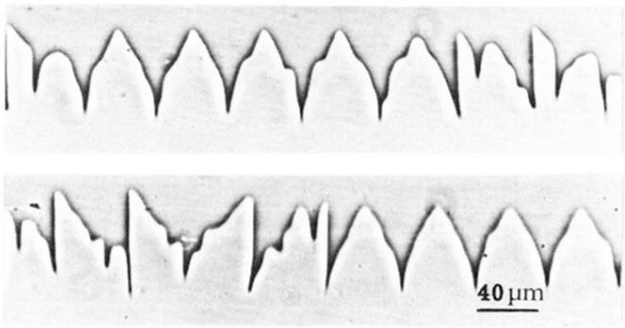

FIG. 4. Nucleation of asymmetric cells in an array of asymmetric cells. Facets are pinned preferentially in the grooves of the widest cells. The tip of the faceted cells is always warmer than that of the symmetric cells. In (a), two neighboring cells have transformed simultaneously into asymmetric cells of the same sign. In (b), the transformation occurred by successive nucleation of two asymmetric cells of opposite signs. A source of asymmetric cells is born.

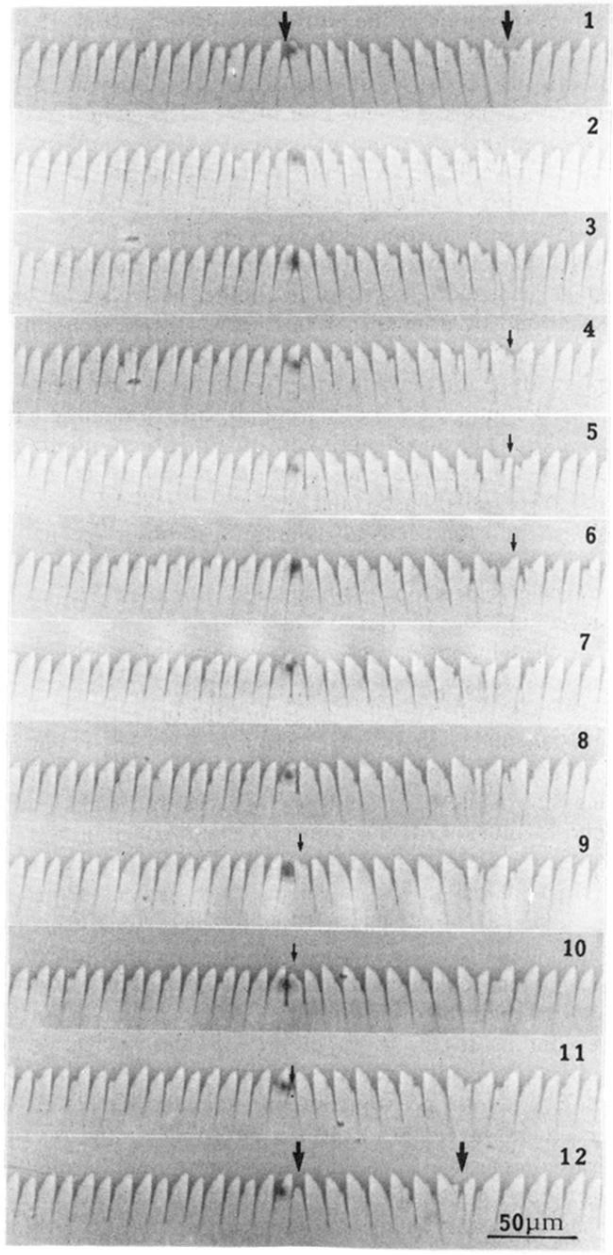

FIG. 5. Source and sink of cells in the asymmetric regime (thick arrows in the photographs). $\Delta T \approx 0.23\,^{\circ}\mathrm{C}$, $G = 63\,^{\circ}\mathrm{C/cm}$, and $V = 2.5\ \mu\mathrm{m/s}$. The time interval between two successive photographs is 10 s. By convention, cells (+) [(−)] have their facet and drift on the right (left). The small arrows in photos (4–6) show the birth of a cell (+) on the nonfaceted side of a cell (−). The arrows (9–11) show the progressive disappearance of a cell (−) in a sink.

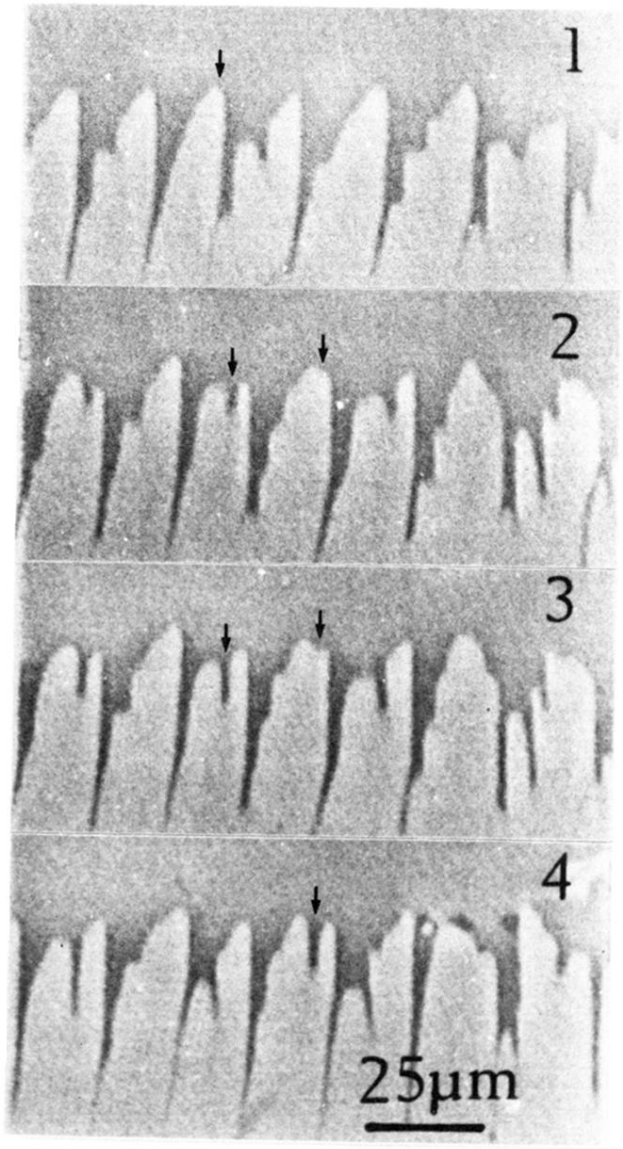

FIG. 8. Tip splitting of the asymmetric cells leading to a chaotic state where the mean wavelength is badly selected. In this nonstationary regime, cells have various shapes and can be symmetric or not with large facet. They change form continually by tip splitting. The photographs have been taken at $t=0(1)$, $t=16$ s (2), $t=20$ s (3), and $t=32$ s (4). $\Delta T \approx 0.3\,^{\circ}\mathrm{C}$, $G=63\,^{\circ}\mathrm{C/cm}$, and $V=3\,\mu\mathrm{m/s}$.

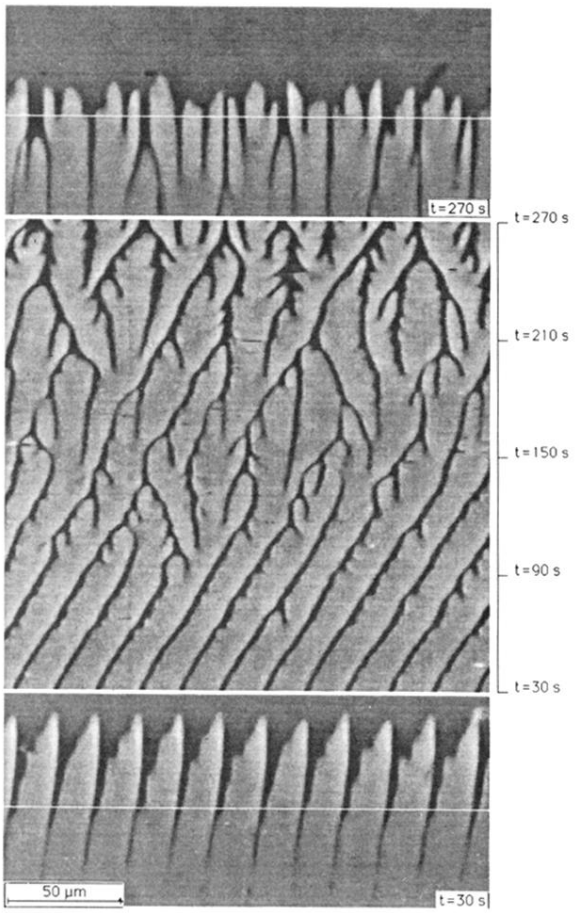

FIG. 9. Spatiotemporal diagram showing the forming of the chaotic regime. At time $t=0$, the velocity has jumped from $V=1.5$ μm/s (domain regime) to $V=2.5$ μm/s (chaotic regime). $\Delta T \approx 0.4\,^{\circ}\mathrm{C}$, $G=63\,^{\circ}\mathrm{C/cm}$. Time is indicated on the right of the diagram which starts 30 s after the jump in velocity. The two photographs show the cellular pattern at the beginning and at the end of the sequence. The white line on each photograph marks the position of the digitalized video line. Note that its position, fixed in the frame of the laboratory, has changed with respect to the tip of the cells. This effect is mainly due to the unavoidable shift of the temperature gradient when the velocity changes.